Biofouling resistant materials based on micro-structured surfaces with liquid-repellent properties

Jitniyom, Thanaphun; Gaddam, Anvesh; Williams, Georgia; Churm, James; Dearn, Karl; Banzhaf, Manuel; De cogan, Felicity; Dimov, Stefan; Gao, Nan

DOI:
10.1002/nano.202300158

Document Version
Publisher's PDF, also known as Version of record

Citation for published version (Harvard):
Jitniyom, T, Gaddam, A, Williams, G, Churm, J, Dearn, K, Banzhaf, M, De cogan, F, Dimov, S & Gao, N 2023, 'Biofouling resistant materials based on micro-structured surfaces with liquid-repellent properties', *Nano Select*, pp. 1-10. https://doi.org/10.1002/nano.202300158

Received: 13 November 2023 | Accepted: 22 November 2023

DOI: 10.1002/nano.202300158

RESEARCH ARTICLE

nano select Open Access WILEY

Biofouling resistant materials based on micro-structured surfaces with liquid-repellent properties

Thanaphun Jitniyom[1] | **Anvesh Gaddam**[1] | **Georgia Williams**[2] | **James Churm**[1] | **Karl Dearn**[1] | **Manuel Banzhaf**[2] | **Felicity de Cogan**[3] | **Stefan Dimov**[1] | **Nan Gao**[1]

[1]Department of Mechanical Engineering, University of Birmingham, Birmingham, UK

[2]School of Biosciences, University of Birmingham, Birmingham, UK

[3]School of Pharmacy, University of Nottingham, Nottingham, UK

Correspondence
Nan Gao, Department of Mechanical Engineering, University of Birmingham, Edgbaston, Birmingham, B15 2TT, United Kingdom.
Email: n.gao@bham.ac.uk

Funding information
Engineering and Physical Sciences Research Council, Grant/Award Number: EP/W010852/1

Abstract

Adhesion of contaminants on various polymer-based devices during fluid-substrate interactions is a common problem that can cause biofouling and corrosion. In this study, hierarchical structures with submicron features on polypropylene (PP), high-density polyethylene (HDPE), and polycarbonate (PC) are fabricated by femtosecond laser ablation. The effect of the hierarchical structures on surface wettability, droplet impact, and bacterial attachment has been examined. Our results demonstrate that the structured polymeric substrates facilitate large contact angles and minimal interfacial adhesion, allowing droplets to roll off at a low angle of inclination below 5°. Further, rendering the hierarchical structures with a low-surface-energy coating can enable the surfaces to exhibit superamphiphobic properties. The low interfacial adhesion properties, as accounted by the large contact angles and small contact angle hysteresis, of such surfaces prevent bacterial attachment and biofilm formation. The findings provide a design principle for creating affordable biofouling resistant surfaces with a submicron topography that can be used for engineering and biomedical devices.

KEYWORDS

anti-biofouling, droplet impact, micro-porous structure, polymer, superhydrophobic surfaces

1 | INTRODUCTION

Super-liquid-repellent surfaces are normally characterized by a high apparent receding contact angle (greater than 140°).[1] For example, droplets of water placed on a superhydrophobic surface will adopt a nearly spherical shape, with the contact angle ranging between 140° (for the receding contact angle) and 180° (for the advancing contact angle).[2] The minimal contact area of a droplet with superhydrophobic surfaces, associated with the spherical shape, allows the droplet to roll off at a low angle of inclination below 10°.[3] Super-liquid-repellent surfaces are typically reliant on nano-structured protrusions coated with a low-surface-energy layer, although surfaces with doubly re-entrant micro-overhangs alone can facilitate large contact angles without being hydrophobized.[4] In any case, it is important to ensure the protrusions are produced in such a way that they prevent the

droplet from penetrating the surface structure. This is essential for the Cassie-Baxter wetting state, where the droplet is partially suspended on top of the surface protrusions.[5–8] Surfaces that enable the droplets to exist in the Cassie-Baxter wetting state can be potentially utilized in various industrial applications, including corrosion protection,[9,10] self-cleaning materials,[11] anti-icing wind turbines,[12] antifouling membranes,[13] directional liquid transportation,[14] and so forth.

For superhydrophobic surfaces that repel droplets of water, which has a high surface tension of around 72 mN m^{-1}, the protrusions can be simple vertical micro-pillars. Such micro-pillars are found on a number of superhydrophobic surfaces in nature, such as lotus leaves,[15] but can also be synthesized by lithography and reactive-ion etching techniques.[16–18] However, there are hardly any known natural surfaces that exhibit a contact angle greater than 150° for low-surface-tension fluids. To achieve a superamphiphobic state that repels both polar and nonpolar fluids, the surface protrusions must be defined with more complex geometries than simple micro-pillars. For example, hierarchically structured porous surfaces have been demonstrated to show superamphiphobic properties.[3,19,20] These porous surfaces consist of randomly aggregated nanoparticles, which, nonetheless, collectively exhibit nanoscopic overhanging structures. Droplets placed on the surfaces will be supported by a combination of overhangs and air cushions. It should also be noted that the air cushion trapped underneath the droplet represents a major characteristic of super-liquid-repellent surfaces. Recent studies have even demonstrated that the absence of an air cushion can significantly boost bacterial adhesion.[21–23] By contrast, the air cushion minimizes the effective contact area between the liquid (e.g., bacteria-containing droplets) and the surface, thus reducing the interfacial adhesion.[24] However, the complex morphology associated with the porous surfaces normally requires expensive or lengthy fabrication processes.

Recently, it has been demonstrated that femtosecond laser ablation can be used to manufacture superhydrophobic surfaces.[25–27] Taking advantage of its high scanning speed and pulse frequency, this technique offers the possibility to generate well-defined micro-structures in a single-step process. Furthermore, the generated surface structure can be rendered with superhydrophobic properties without the need of additional low-surface-energy coating, which is attributed to the adsorption of long-chain hydrocarbons (organic compounds) from air[28] or decomposition of carbon dioxide into carbon subjected to the laser treatment. [29] As such, femtosecond laser ablation can enable high throughput processing of complex 3D microstructures for superhydrophobic surfaces.

In this work, we make use of femtosecond laser ablation to directly fabricate hierarchical structures that facilitate super-liquid-repellence on various polymeric sheets (Figure 1), including polypropylene (PP), high-density polyethylene (HDPE) and polycarbonate (PC). Droplets of water on these polymeric substrates with laser-induced topographies can roll off at a low angle of inclination below 5°, implying minimal interfacial adhesion. We also note that the PC surfaces decorated with submicron structures can be further treated with a low-surface-energy coating to achieve superamphiphobicity. In addition, our studies demonstrate that the structured surfaces suppress bacterial attachment, showing potential applications in preventing biofilm formation and growth.

2 | RESULTS AND DISCUSSION

The topographies of the resultant surfaces directly produced by laser ablation are shown in Figure 1. The microscale patterns are distributed evenly on all three types of substrate surfaces. Specifically, the resultant morphology on the PP surface (Figure 1B–D) was composed of sub-micrometer scale textures that exhibited spherical shapes on top of microscale clusters. One could identify a similar morphology on the HDPE surface (Figure 1E–G), which exhibited more microscale pores than the PP surface. Further, the PC (Figure 1H–J) surface exhibited distinct hierarchical features that combine microscale protrusions and submicron structures, implying that the PC surface had a greater capacity for entrapping air pockets. Nonetheless, it should be noted that the fabrication process led to many pores or cavities on all of these surfaces. The 3D profiles of each surface, with the arithmetical mean height (*Sa*) and the developed interfacial area ratio (*Sdr*), are shown in Figure 2. The measured values of *Sa* for PP and HPDE surfaces were 1.09 and 0.98, respectively, while PC surfaces featured the highest roughness of 1.87. Further, the *Sdr* of PC was 49.78%, which is significantly higher than that of HDPE (12.13%) and PP (16.67%). This indicates that the additional surface area contributed by the texture as compared to the planar definition area on the PC surface was higher than PP and HDPE surfaces, consistent to the feature revealed by the SEM images.

The contact angles were influenced by the pattern of the surfaces (Figure 3), depending on the material property of each polymer substrate. For the untreated PP, HDPE and PC surfaces, the static water contact angles (WCA) were around 103°, 102° and 92°, respectively. However, the contact angle hysteresis (CAH), defined as the difference between the advancing contact angle (θ_{adv}) and the receding contact angle (θ_{rec}), is greater than 10° for all three types of bare surfaces, as shown in Table 1.

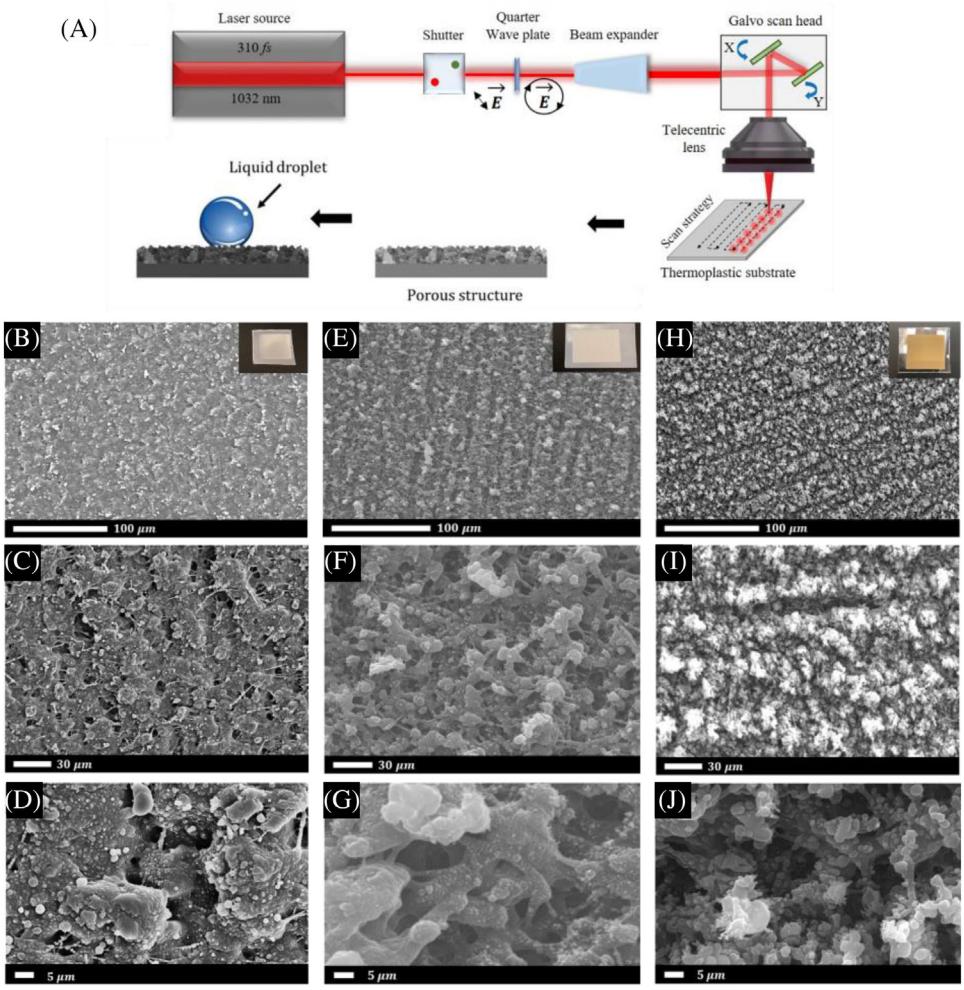

FIGURE 1 A, Diagram of the preparation process for the surfaces by steering a femtosecond laser beam directly onto a substrate. SEM images of the PP (B–D), HDPE (E–G) and PC (H–J) surfaces after laser ablation under different magnifications.

Roughening the surfaces with a femtosecond laser (Figure S1) resulted in a significant increase in the WCA for all three types of polymeric substrates. Indeed, the contact angle hysteresis became far smaller after the laser ablation, being around 9°, 9° and 4° for the PP, HDPE and PC structures, respectively. In addition, coating the surfaces with (1H,1H, 2H, 2H-perfluorooctyl) silane (FAS) made the contact angle hysteresis exhibit similarly low values of around 5°. Hence the textured surfaces with the low-energy coating are now denoted as superhydrophobic, because of their large water contact angles and small contact angle hysteresis.

TABLE 1 Advancing contact angle (θ_{adv}), receding contact angle (θ_{rec}) and contact angle hysteresis (θ_h) of water droplets on different types of surfaces.

Surface types	θ_{adv}	θ_{rec}	θ_h
Bare PP	104.8 ± 0.7°	85.29 ± 1.2°	19.46 ± 1.1°
PP rough	148.37 ± 3.8°	139.17 ± 2.8°	9.19 ± 1.5°
PP rough +FAS	150.73 ± 2.9°	146.15 ± 4.2°	4.58 ± 1.7°
Bare HDPE	108.6 ± 4.6°	93.13 ± 1.7°	15.48 ± 3.7°
HDPE rough	152.18 ± 0.5°	142.8 ± 1.6°	9.37 ± 1.5°
HDPE rough + FAS	152.09 ± 2.1°	146.47 ± 3.7°	5.62 ± 1.7°
Bare PC	104.02 ± 1.8°	88.37 ± 1.9°	15.64 ± 1.4°
PC rough	148.7 ± 2.2°	144.88 ± 2.1°	3.82 ± 1.5°
PC rough + FAS	152.29 ± 1.2°	147.84 ± 0.9°	4.44 ± 0.9°

In addition, the wettability of the surfaces has been probed against hexadecane which has a lower surface tension (around 27 mN m^{-1}) than water.[30] As shown in Figure 3, both the bare substrates and the laser-roughened substrates (denoted as "rough") were highly wettable by hexadecane, with low contact angles (smaller than 20°) and experimentally unmeasurable contact angle hysteresis. Using (1H,1H, 2H, 2H-perfluorooctyl) silane for this instance was advantageous to lower surface energy and prevented the liquid from spreading on the surfaces. For example, the receding contact angles (Table 2) of hexadecane increased to around 81° and 102°, respectively, on

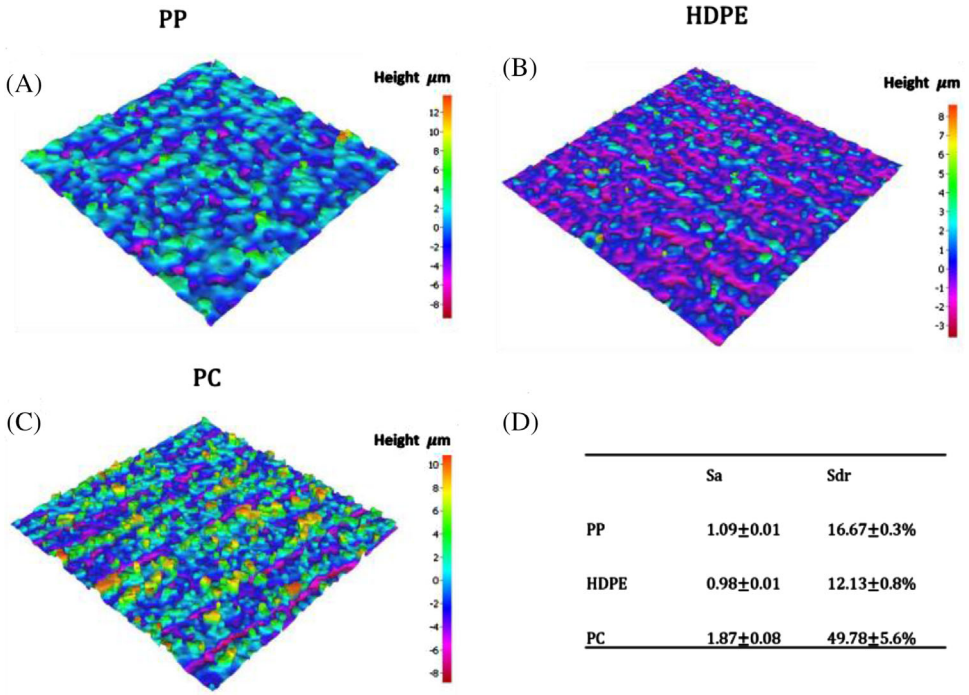

	Sa	Sdr
PP	1.09±0.01	16.67±0.3%
HDPE	0.98±0.01	12.13±0.8%
PC	1.87±0.08	49.78±5.6%

FIGURE 2 A–C, 3D profiles of the topographies on PP, HDPE and PC, respectively. D, Measured roughness (*Sa*) and developed interfacial area ratio (*Sdr*) of each surface.

roughened PP and HDPE surfaces coated with (1H,1H, 2H, 2H-perfluorooctyl) silane. In particular, the contact angle of hexadecane on PC reached 140°, indicating that the low-surface-energy coating enabled the roughened PC surfaces to become superamphiphobic. Furthermore, the contact angle hysteresis of hexadecane on the treated surfaces was significantly decreased to 33° for PP, 26° for HDPE and 12° for PC.

A range of droplet impact experiments were carried out to monitor the behaviors of the droplets when colliding with the surfaces. The snapshots of the droplet impacts were captured at a frame rate of 2000 fps. Figure 4 indicates that the structured surfaces directly obtained from laser ablation can repel the impacting water droplets (9 μL). This is in contrast with the bare substrates characterized by the large contact angle hysteresis, which did not allow the impacting droplets to bounce at all from the release height of 15 mm ($v = 0.54$ m s^{-1}, $We = 10.45$, Videos S7–S15). Specifically, the impacting droplets spread rapidly (within 4.5 ms) to reach the maximum extension upon hitting the bare substrates, assuming a pancake shape. This was followed by a retraction phase toward the impact point before the droplet finally stabilized, adhering firmly to the surface. On the other hand, the droplets rebounded upon impacting the HDPE and PC surfaces with hierarchical structures that entrapped air pockets, indicating the surfaces featured low adhesion. However, for the PP surfaces directly obtained from laser ablation, of which the surface morphology was dominated by the microscopic texture, only a partial rebound was observed. Nonetheless, applying the low-surface-energy coating on the surfaces made it possible for the impacting droplets to bounce multiple times before the droplets stabilized on the surfaces. It was also possible for the droplets to roll off from the surfaces with small tilting angles. For surfaces resultant from direct femtosecond laser ablation, water droplets rolled off at a tilting angle of around 10°. In contrast, water droplets rolled off from the superhydrophobic and superamphiphobic surfaces at smaller tilting angles of 2–4° (Videos S1–S6).

TABLE 2 Advancing contact angle (θ_{adv}), receding contact angle (θ_{rec}) and contact angle hysteresis (θ_h) of hexadecane droplets on different types of surfaces.

Surface types	θ_{adv}	θ_{rec}	θ_h
PP rough + FAS	113.8 ± 0.8°	80.9 ± 1.5°	32.9 ± 1.7°
HDPE rough + FAS	127.9 ± 0.2°	102 ± 0.1°	25.9 ± 0.2°
PC rough + FAS	152.4 ± 0.8°	140.2 ± 0.7°	12.2 ± 1°

To explore the application of the liquid-repellent surfaces, we have also tested their antifouling capacities. Figures 5 and 7 depict the results of the antifouling test using laser scanning confocal microscopy (LSCM) and SEM. The detailed test procedures of this study can be found in Section 4. In brief, the bacterial attachment for the bare substrates was studied as a baseline to compare

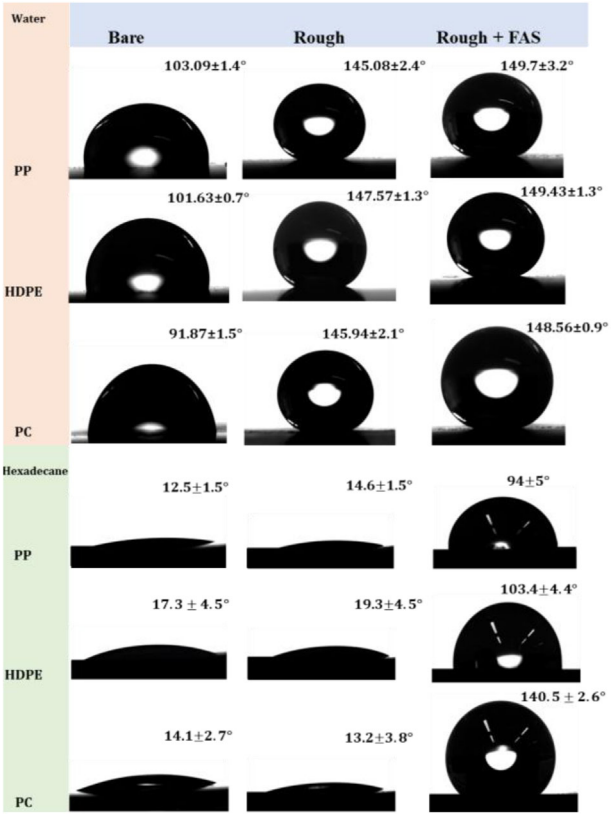

FIGURE 3 Contact angles of water and hexadecane droplets on different surfaces. The untreated substrates are denoted as "Bare", the laser-ablated substrates are denoted as "Rough", and the laser-ablated substrates further coated with (1H,1H, 2H, 2H-perfluorooctyl) silane are denoted as "Rough + FAS".

with the treated surfaces. The fluorescent samples of bare surfaces (Figure 5A–C) display large colonies of the fluorescent bacteria. In particular, the attached bacteria could even form colonies, for example, on the bare PC surface, instead of individual bacteria. By contrast, the textured surfaces (Figure 5D–F) of HDPE, PP and PC obtained from direct laser ablation were covered with individual bacteria, forming significantly less coverage in comparison with the untreated bare surfaces. Notably, there were only sparse and isolated bacteria on the coated superhydrophobic and superamphiphobic surfaces (Figure 5G–I) which had small contact angle hysteresis (< 5°). Indeed, bacterial attachment was consistently prevented on the textured surfaces, as evidenced by the confocal microscopy and SEM images. It is thus noted that the low droplet adhesion of these surfaces, regardless of the presence of low-surface-energy coating, led to minimal levels of bacterial attachment in comparison with the control surfaces (bare substrates). This is likely resultant from the presence of entrapped air pockets, which remained at the apparent solid/liquid interface while the surfaces were exposed to bacterial suspension, creating a lower actual bacterial contact area. Furthermore, we quantified bacterial attachment by counting the number of bacteria on the LSCM images using ImageJ (Tables S2–S4 and Figures S2–S11). Figure 6 shows the coverage of bacteria that were attached to the surfaces, providing a quantitative antibiofouling effect. Specifically, the coverage decreased to 1.07 ± 0.5% on the laser-roughened PP surface and 0.15 ± 0.1% on the coated superhydrophobic PP surface from 6 ± 4.1% on the bare PP surface. The superhydrophobic HDPE surface reached 0.88 ± 0.73% which is smaller than the bare (4.87 ± 1%) and the laser-roughened HDPE (2.41 ± 1.4%) surfaces. Furthermore, the coverage of bacteria on the superamphiphobic PC surface was merely 0.03 ± 0.02%, significantly lower than that on the bare (25.95 ± 3.5%) and laser-roughened PC surfaces (5.53 ± 1.8%). We have also observed a similar trend from the SEM images (Figure 7), where the bare substrates showed more coverage of colonies than the superhydrophobic and superamphiphobic surfaces. The purpose of this investigation was to demonstrate whether the liquid repellent surfaces were effective in delaying or preventing bacterial attachment. Indeed, several studies[8,10] have shown that superhydrophobic surfaces exhibiting the Cassie-Baxter wetting state are less susceptible to bacterial attachment than hydrophobic or hydrophilic counterparts, because of the presence of air pockets entrapped within the surface structure.[22,23] Our results indicate that the surface coverage on the textured surfaces was lower, regardless of the existence of the low energy coating, than that on bare surfaces. We note that the variation in the coverage between different samples gives rise to the error bars. Nonetheless, overall, the textured surfaces with liquid-repellent properties can effectively reduce bacterial attachment by facilitating minimal interfacial contact.

3 | CONCLUSION

In summary, our main objective was to develop structured surfaces with super-liquid-repellent properties, and to evaluate their antifouling capacity. Femtosecond laser ablation was utilized in this work to create such structures on various polymeric substrates, which facilitated minimal adhesion for droplets of water and/or hexadecane. Water droplet bouncing and rolling under different surface conditions were investigated to further characterize the wettability of the fabricated surfaces. Specifically, superhydrophobic wetting properties were realized by generating hierarchical structures through femtosecond laser ablation on the polymeric substrates. Additional modification of the structures with low-surface-energy coating made it possible for the surfaces to exhibit superamphiphobic properties. Notably, our findings demonstrated that the

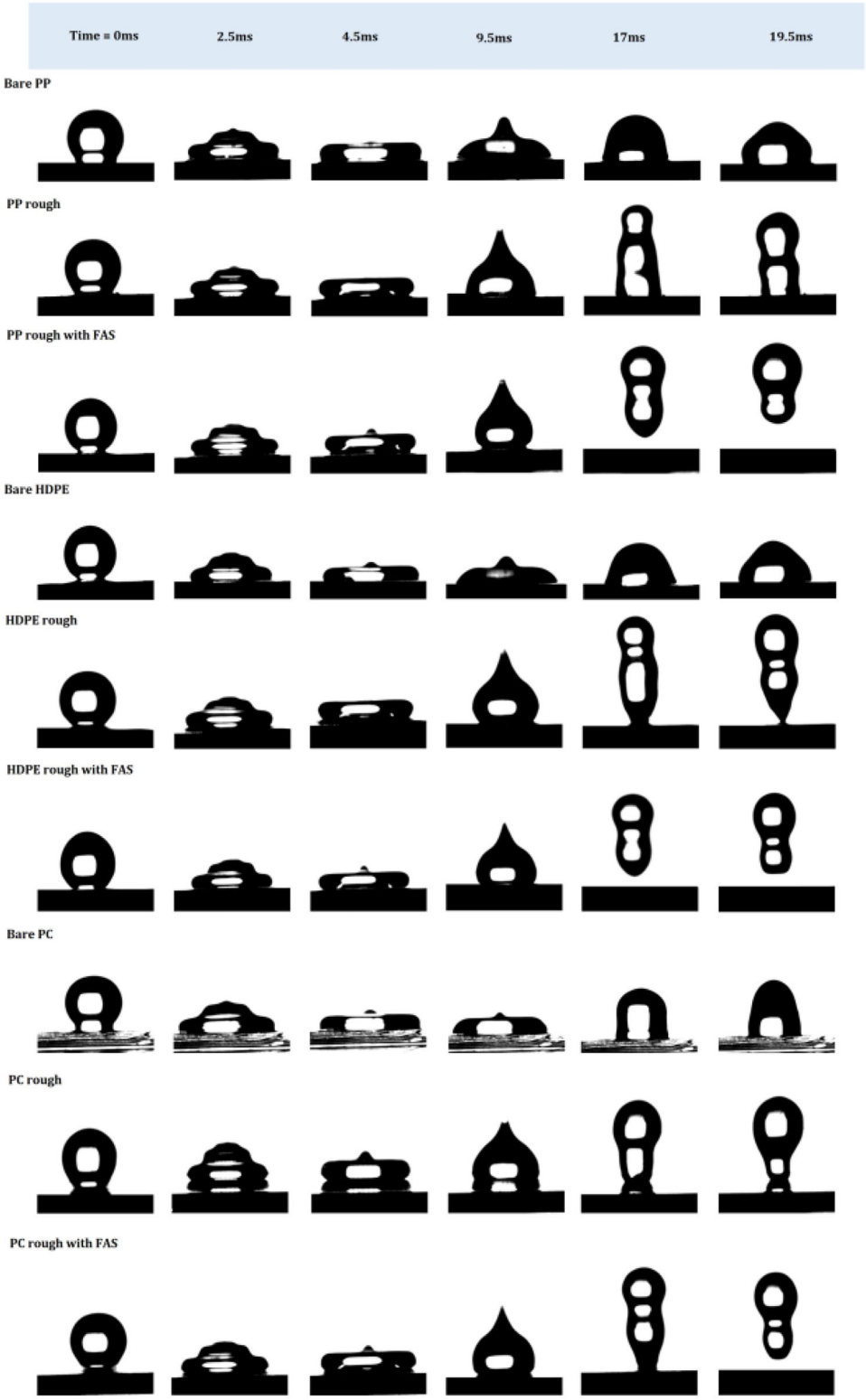

FIGURE 4 Snapshots of water droplets impacting the surfaces recorded using a high-speed camera. The frame rate is 2000 fps, velocity at approximately 0.54 m s^{-1} and $We = 10.45$. The volume of the droplet is 9 μL.

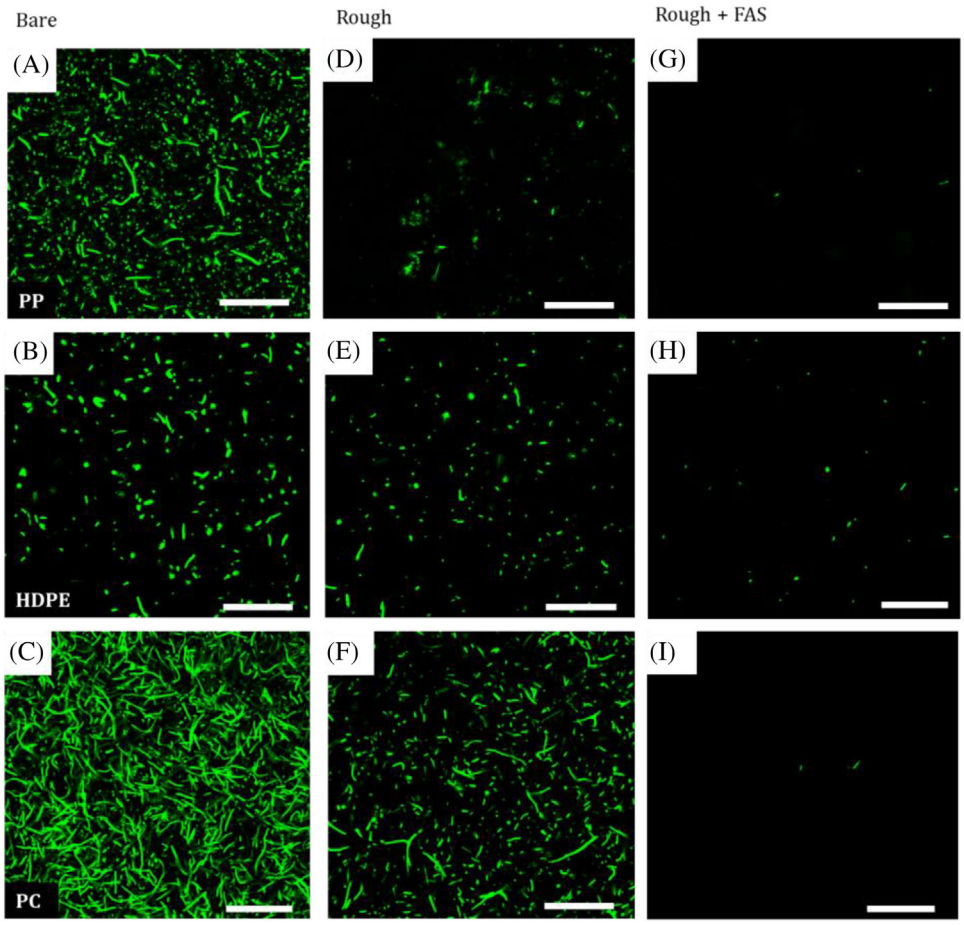

FIGURE 5 Images investigating *E. coli* bacteria expressing green fluorescent protein (GFP) (green spots) under LSCM. The bacterial suspension was incubated on the polymeric surfaces of PP, HDPE and PC: (A–C) bare substrates, (D–F) laser-ablated substrates and (G–I) laser-ablated substrates coated with FAS. *E. coli* expressing GFP was visualized at an excitation wavelength of 488 nm. The scale bars are around 50 μm.

hierarchically structured surfaces with liquid repellent properties significantly reduced bacterial attachment, which was even more pronounced for the superamphiphobic surfaces. Such results are attributed to the presence of air cushions for the tested surfaces. These findings are useful for understanding bacterial attachment in real life and, hence, the design of anti-biofouling surfaces.

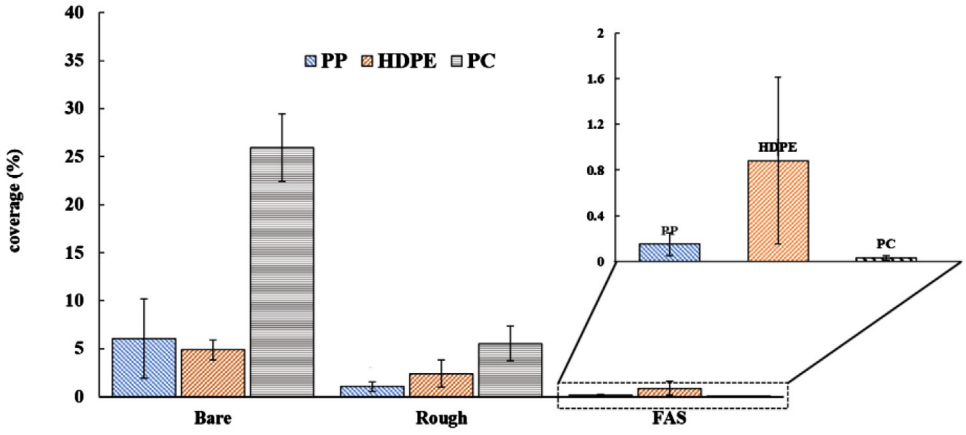

FIGURE 6 The coverage of bacterial attachment on the surfaces.

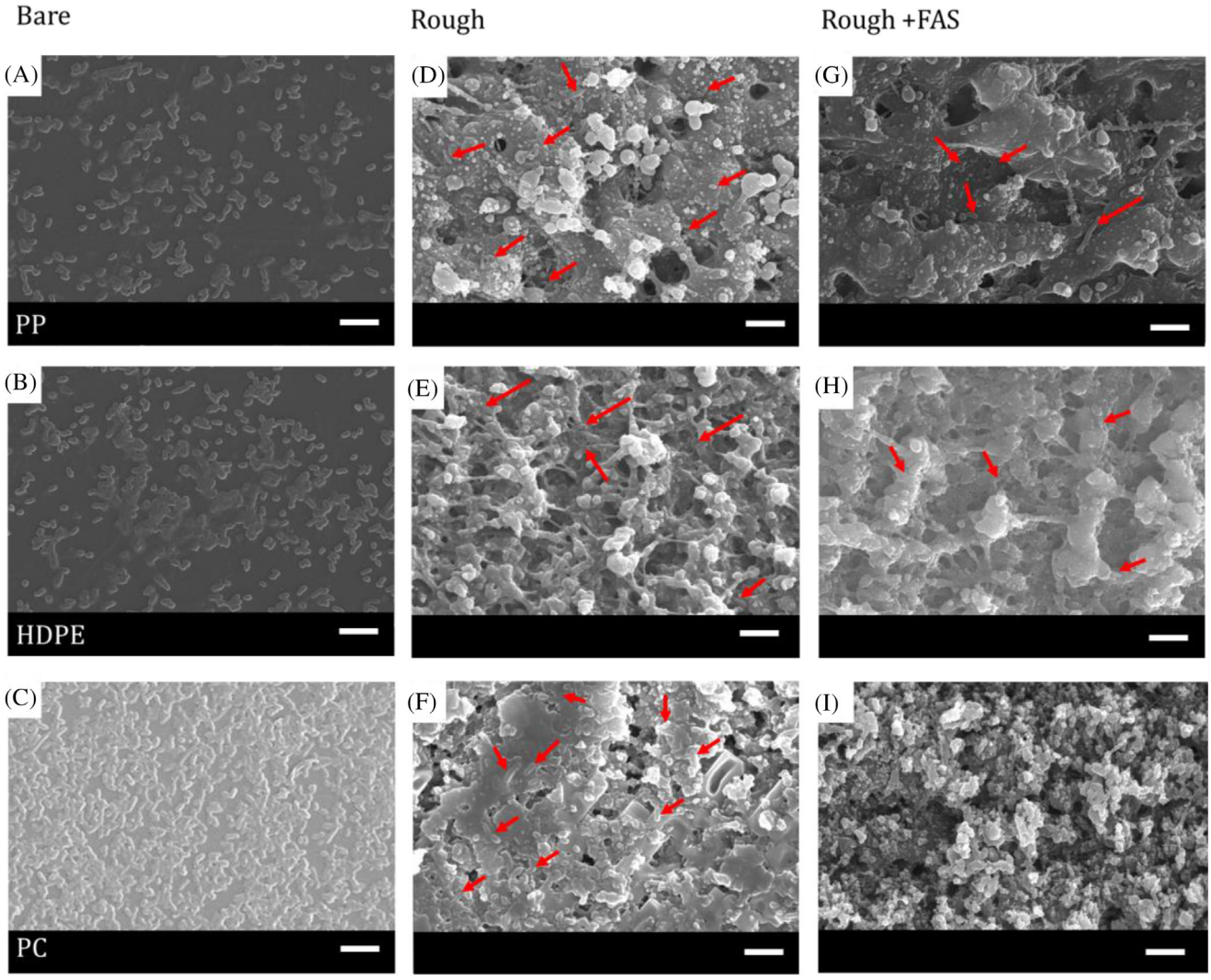

FIGURE 7 SEM images investigating *E. coli* bacteria on different surfaces. The bacterial suspension was incubated on the polymeric surfaces of PP, HDPE and PC: (A–C) bare substrates, (D–F) laser-ablated substrates and (G–I) laser-ablated substrates coated with FAS. The red arrows are used to indicate where the attached bacteria are. The scale bars are around 10 μm.

4 | EXPERIMENTAL SECTION

Fabrication of micro-structures on polymeric surfaces

PP, HDPE and PC sheets with a thickness of 1 mm were purchased from Sigma Aldrich and cut to individual pieces with a size of 25 × 25 mm. The micro-structures on these thermoplastic substrates were fabricated using a femtosecond laser machining workstation (LS5, LASEA, Belgium). The beam delivery system with its components is illustrated in Figure 1. Briefly, the system is equipped with an Ytterbium-doped femtosecond laser source (Satsuma, Amplitude Systems), which operates at a near infrared wavelength (λ) of 1032 nm and has a pulse duration of 310 fs. The maximum pulse repetition rate (f) and average power (P) of the laser are 500 kHz and 5 W, respectively. Also, it includes a half wave plate, a beam expander and a telecentric focusing lens of 100 mm to obtain a linearly polarized (s-type) beam with a spot diameter (2ω) of 60 μm at focus. A 3D galvo scan head is used to steer beam at a speed (v) of up to 2000 mm s^{-1}. The thermoplastic substrates were positioned on a motorized stage normal to the incident laser beam in the experiments. All the substrates were processed with a fixed pulse fluence ($\varphi_0 = P/\pi\omega^2 f$) of 47 mJ cm^{-2} and a scanning speed of 1000 mm s^{-1} and a pulse repetition rate of 500 kHz to produce the micro-structures. The pulse-to-pulse distance ($d = v/f$) was 2 μm. Furthermore, the hatch distance (h) between successive scan lines (see Figure 1) was maintained at 2 μm during the experiments. Overall, the micro-structures were achieved as a result of irradiating the polymer substrates with an accumulated fluence ($\varphi = P/fdh$) of 135.5 J cm^{-2}. The overall processing time of 25 × 25 mm area with the applied settings was 5 minutes and 15 seconds per substrate.

All the surfaces were placed in a vacuum desiccator at room temperature with 30 μL of (trichloro (1H,1H, 2H, 2H-perfluorooctyl) silane (97%, Sigma Aldrich) on a glass slide next to the surfaces for 90 minutes to lower the surface energy. We note that the surfaces were modified within 1 week of laser ablation. After the coating process, the surfaces were removed from the vacuum desiccator and left overnight or 20 hours, before measurement of the contact angle and contact angle hysteresis. The topography of the laser-ablated surfaces was observed using SEM (Zeiss EVO 10) and 3D profilometry (Alicona). A layer of gold coating was applied before employing the SEM.

Wettability characterization

Contact angles and contact angle hysteresis were measured by using a Data-Physics OCA 15 contact angle goniometer. Droplets of 6 μL were deposited on the substrates. The measurement was repeated on five different areas of at least 3 samples for each surface type to obtain an average value of the contact angles. The advancing and receding contact angles were measured by increasing/decreasing droplet volumes, and each measurement was repeated 5 times on 3 samples of each type of the surfaces (Table S1). The droplet impact was imaged using a high-speed camera (Photron, FASTCAM Mini UX100; image analysis software PFV4). The volume of water droplets was 9 μL, the dimensionless Weber number was calculated as follows: $We = (\frac{\rho d v^2}{\sigma})$ where ρ is density, d is liquid diameter, v is velocity (m s^{-1}) and σ is surface tension (N m^{-1}).[31] The frame rate of the high-speed camera is 2000 fps with a maximum resolution of 1280 × 1024. The height between the electronic syringe and the top of the surfaces was at 15 mm.

Bacterial attachment testing

Escherichia coli (E. coli) BW25113 expressing green fluorescent protein (GFP) was cultured in 5 mL of sterile Lysogeny broth (LB) overnight at 37°C for around 18 hours with shaking (180 rpm) before being adjusted to around 1×10^9 (colony-forming units) CFU mL^{-1}. Bacterial suspensions of 120 μL were arrayed across each of the surfaces of fixed sizes of 10 × 10 mm. It should be noted that a bacterial suspension is a cell culture whereby colonies of bacterial cells are surrounded by growth medium which allows them to function and multiply. Arraying bacterial suspensions across the surface materials enabled bacterial colonies to be in contact with the surface whilst still enabling the bacteria to receive the appropriate nutrients from the medium. The amount of bacterial suspension added to each surface was to ensure that there was full coverage of the surface by the bacterial suspension (approximately 2–3 mm thickness of the bacterial suspension on top of the surface). The surfaces were incubated with the bacterial suspensions for 20 hours at room temperature (approx. 25°C). After this, the overnight culture medium was removed by tilting the surfaces, which were then gently washed with phosphate buffered saline (PBS) (up to 40 μL). In the final step, all surfaces were covered with glass cover slips before using the confocal laser scanning microscope (TCS SP8, HC PL APO CS2 40×/1.40 oil objective) to observe the bacteria on the surfaces. 1–2 drops of immersion oil (*Immersol* 518 F) were added to the top of the glass cover slip.

Scanning electron microscopy (SEM)

After 20 hours of exposure to the bacterial media, the surfaces were imaged with a scanning electron microscope (Zeiss EVO 10). The samples were washed with 40 μL of phosphate buffer solution (PBS) to remove residual media. After the washing procedure, glutaraldehyde 2.5% (v/v) as a fixative solution was added to the sample surfaces to fix the cells prior to SEM imaging. Glutaraldehyde was pipetted from the side of the sample surfaces to prevent any cells from being washed off. The samples were then incubated at room temperature for 30 minutes. After this, the surfaces were rinsed with PBS and subsequently water/ethanol mixtures for serial drying at room temperature. The concentrations of ethanol in the mixtures used for this process were in the range of 50%, 55%, 60%, 75%, 80%, 90%, and 100%. The samples were incubated with each concentration for 15 minutes and then replaced with the next solution that had a higher concentration of ethanol. The final step was to leave the samples with the water/ethanol mixtures to evaporate completely, allowing them to be ready for SEM imaging. Gold was sputter-coated onto the dried surfaces to increase imaging contrast.

ACKNOWLEDGEMENTS

We thank the Engineering and Physical Sciences Research Council (EPSRC) for support under the grant of EP/W010852/1.

CONFLICT OF INTEREST STATEMENT

The authors declare no conflict of interest.

DATA AVAILABILITY STATEMENT

The data that support the findings of this study are available in the supplementary material of this article.

ORCID

Nan Gao https://orcid.org/0000-0001-7510-2886

REFERENCES

1. H. J. Butt, N. Gao, P. Papadopoulos, W. Steffen, M. Kappl, R. Berger, *Langmuir* **2016**, *33*, 107

2. F. Schellenberger, N. Encinas, D. Vollmer, H. J. Butt, *Phys. Rev. Lett.* **2016**, *116*, 2
3. H. Teisala, F. Geyer, J. Haapanen, P. Juuti, J. M. Makela, D. Vollmer, H.J Butt, *Adv. Mater.* **2018**, *30*, 14
4. L. Liu, C. J. Kim, *Science* **2014**, *346*, 1096
5. B. D. Cassie, S. Baxter, *Trans. Faraday Soc.* **1944**, *40*, 546
6. P. Roach, N. J. Shirtcliffe, M. I. Newton, *Soft Matter* **2008**, *4*, 224
7. D. Bonn, J. Eggers, J. Indekeu, J. Meunier, E. Rolly. *Rev. Mod. Phys.* **2009**, *81*, 739
8. H. Yildirim Erbil, *Langmuir*, **2020**, *36*, 2493
9. Y. Jiang, C.-H. Choi, *Adv. Mater. Interfaces* **2021**, *8*, 2001205.
10. M. Liravi, H. Pakzad, A. Moosavi, A. Nouri-Borujerdi, *Lsevier B.V.* **2020**, *140*, 105537
11. R. Furstner, W. Barthlott, C. Neinhuis, P. Walzel, *Langmuir*, **2005**, *21*, 956
12. O. Parent, A. Ilinca, *Cold Reg. Sci. Technol.* **2011**, *65*, 88
13. D. Rana, T. Matsuura, *Chem. Rev.* **2010**, *110*, 2448
14. B. Hu, Z. Duan, B. Xu, K. Zhang, Z. Tang, C. Lu, M. He, L. Jiang, H. Liu, *J. Am. Chem. Soc.* **2020**, *142*, 6111
15. W. Barthlott, C. Neinhuis, *Planta* **1997**, *202*, 8
16. L. Gao, T. J. McCarthy, *Langmuir* **2006**, *22*, 6234
17. Y. Kwon, N. Patankar, J. Choi, J. Lee, *Langmuir* **2009**, *25*, 6129
18. S. Wooh, J. H. Koh, S. Lee, H. Yoon, K. Char, *Adv. Funct. Mater.* **2014**, *24*, 5550
19. X. Deng, L. Mammen, H. J. Butt, D. Vollmer, *Science* **2012**, *335*, 67
20. Q. Sun, D. Wang, Y. Li, J. Zhang, S. Ye, J. Cui, L. Chen, Z. Wang, H. J. Butt, D. Vollmer, X. Dang, *Nat. Mater.* **2019**, *18*, 936
21. N. Encinas, C. Y. Yang, F. Geyer, A. Kaltbeitzel, P. Baumli, J. Reinholz, H. J. Butt, D. Vollmer, *ACS Appl. Mater. Interfaces* **2020**, *12*, 21192
22. G. B. Hwang, K. Page, A. Patir, S. P. Nair, E. Allan, I. P. Parkin, *ACS Nano*, **2018**, *12*, 6050
23. J. Jiang, H. Zhang, W. He, T. Li, H. Li, P. Liu, M. Liu, Z. Wang, Z. Wang, X. Yao, *ACS Applied Materials & Interfaces*, **2017**, *9*, 6599
24. N. Gao, F. Geyer, D. Pilat, S. Wooh, D. Vollmer, H. J. Butt, R. Berger, *Nat. Phys.* **2018**, *14*, 191
25. J.-M. Romano, A. Garcia-Giron, P. Penchev, S. Dimov, *Appl. Surf. Sci.* **2018**, *440*, 162
26. J. Yong, J. Huo, Q. Yang, F. chen, Y. Fang, X. Wu, L. Liu, X. Lu, J. Zhang, W. Hou, *Adv. Mater. Interfaces* **2018**, *5*, 1701479
27. G. Schnell, C. Polley, R. Thomas, S. Bartlinh, J. Wagner, A. Springer, H. Seitz, *J. Colloid Interface Sci.* **2023**, *630*, 951
28. J. Long, M. Zhong, H. Zhang, P. Fan, *J. Colloid Interface Sci.* **2015**, *441*, 1
29. A.-M. Kietzig, S. G. Hatzikiriakos, P. Englezos, *Langmuir* **2009**, *25*, 4821
30. L. I. Rolo, A. I. Caco, A. J. Queimada, I. M. Marrucho, J. A. P. Coutinho, *J. Chem Eng.* **2002**, *47*, 1442
31. J. Peakall, J. Warburton, *J. Hydrol.* **1996**, *35*, 199

SUPPORTING INFORMATION

Additional supporting information can be found online in the Supporting Information section at the end of this article.

How to cite this article: T. Jitniyom, A. Gaddam, G. Williams, J. Churm, K. Dearn, M. Banzhaf, F. de Cogan, S. Dimov, N. Gao, *Nano Select* **2023**, 1. https://doi.org/10.1002/nano.202300158